J. Biochem. **139**, 421–430 (2006)
doi:10.1093/jb/mvj047

Probing the Catalytic Center of Porcine Aminoacylase 1 by Site-Directed Mutagenesis, Homology Modeling and Substrate Docking

Zhigang Liu, Zhongliang Zhen, Zhenyu Zuo, Yingliang Wu, Aifu Liu, Qingming Yi and Wenxin Li*

National Key Laboratory of Virology, College of Life Sciences, Wuhan University, Wuhan 430072, P.R. China

Received August 25, 2005; accepted December 20, 2005

Three-dimensional structural models of porcine aminoacylase 1 (pACY1) were constructed by homology modeling and aligning the structures of members of the M20 peptidase family. After energy minimization and quality evaluation, the best model from the homology modeling was chosen for docking with the best substrate (*N*-acetyl-L-methionine). The most reasonable binding mode was found among a large number of predicted complexes by using clustering analysis and screening with expert knowledge. Structural analysis revealed that the zinc ion is not likely to bind to the substrate, and that Arg^{348} and Glu^{146} play vital roles in binding and catalysis. In the site-directed mutagenesis experiments, mutation of His^{79}, Asp^{112}, Glu^{147}, Arg^{348}, and Glu^{146}, resulted in significant reductions of specific activity, while the wild-type pACY1 overexpressed in Rosetta™ (DE3) had almost as high a specific activity as the native enzyme. On the basis of these observations, we proposed a revised catalytic mechanism for this metalloenzyme.

Key words: aminoacylase 1, catalytic center, docking, energy minimization, homology modeling, site-directed mutagenesis.

Abbreviations: ACY1, aminoacylase 1; pACY1, porcine aminoacylase 1; hACY1, human aminoacylase 1; CPG2, *Pseudomonas* strain carboxypeptidase G2; DAPE, succinyldiaminopimelate desuccinylase; nmDAPE, *Neisseria meningitidis* mc58 succinyldiaminopimelate desuccinylase; AARE, acylamino acid–releasing enzyme; RMSD, root-mean-square deviation; PepT, amino tripeptidase T; PepV, peptidase V.

Aminoacylase 1 (N^a-acyl-L-amino acid aminohydrolase, EC 3.5.1.14; ACY1) is a soluble homodimeric zinc-containing metalloprotein comprised of 812 amino acids and has no intramolecular disulfide bond (*1*). It belongs to the M20 peptidase family and catalyzes the deacylation of *N*-acylated L-amino acids other than aspartic acid and proline (*2*).

ACY1 is widely distributed in various tissues, and its physiological function remains unclear. It has been suggested to be involved in the catabolism of N-terminally acetylated proteins in combination with acylamino acid-releasing enzyme (AARE) [EC 3.4.19.1], which catalyzes the release of the terminal acetyl amino acid from peptide (*3*). The recent finding that the region 3p21 of human chromosome 3 including genes for both ACY1 and AARE is deleted in human carcinoma cells further supports the notion that these two enzymes play a critical role in deacetylation of N-terminally acetylated proteins (*4*, *5*). It has been suggested that accumulation of unknown *N*-acetylated peptide growth factors in the absence of ACY1 and AARE induces these carcinoma cells to proliferate (*6*). Therefore, ACY1 may be a potential therapeutic target for anti-cancer drugs. ACY1 also has significant industrial uses and has been applied for the preparation L-amino acids (*7*).

Although many studies have addressed the biochemical properties of ACY1, the integrated three-dimensional structure or enzyme-substrate complex structure of this protease remains unknown. Because attempts to crystallize this enzyme have not been successful, information regarding its structure is scanty and fragmented. However, some progress has been made recently. For example, the crystal structure of the zinc-binding domain of the T347G mutant of human ACY1 (hACY1) was elucidated (*8*), and the dimeric structure of porcine ACY1 (pACY1) was probed by mass spectrometric and modeling procedures (*9*). These works greatly improved our understanding of ACY1 structure and catalysis. But the exact role of the zinc ion, an essential metal for the catalytic activity of this enzyme, is obscure. It has been proposed that the zinc ion directly participates in substrate binding and catalysis (*10*, *11*), but nuclear magnetic relaxation studies suggested this metal ion only plays a purely structural role (*12*). Information on the enzyme-substrate complex structure of pACY1 is critical for the understanding of this enzyme's catalytic mechanism and substrate specificity.

In this article, we constructed a homology model for pACY1 by using the 3D structures of T347G mutant of hACY1, *Pseudomonas* strain carboxypeptidase G2 (CPG2), and *Neisseria meningitidis* mc58 succinyldiaminopimelate desuccinylase (nmDAPE), which have sequence homologies of 89%, 20% and 23% respectively with pACY1. We further characterized the catalytic center by docking this model with *N*-acetyl-L-methionine, the best substrate

*To whom correspondence should be addressed. Tel: +86-27-68752831, Fax: +86-27-68759146, E-mail: liwxlab@whu.edu.cn

Table 1. **Forward versions of mutagenic primers.**

Mutant	Predicted role in pACY1	Oligonucleotide sequence[a]
H79A	Zinc binding	5′-CCATCTTGCTCAACTCCGCAACAGATGTGGTGCCTGTC-3′
D112A	Zinc binding	5′-CAGGGGCGCCCAGGCAATGAAGTGCGTCAG-3′
E147A	Zinc binding	5′-CTTTGTGCCAGATGAGGCTGTTGGAGGTCACCAAGG-3′
E146A	General base	5′-ACCTTTGTGCCAGATGCTGAGGTTGGAGGTCACC-3′
E174A		5′-TTGCCCTGGATGCAGGCCTAGCCAGC-3′
H205L		5′-GGAAGCCAGGGCTTGGCTCGCGCTTC-3′
N261A		5′-GGTGGCGTGGCCTATGCAGTCGTTCCTGCCACC-3′
R274A		5′-GTGCCTGCTTTGACTTCGCAGTAGCACCGGATGTGGAC-3′
R348A	Catalytic	5′-CTGCTTCCACTGACGCCGCATATATTCGTGCGGCGG-3′
E309H		5′-GTTCAGAGGTGGATGCACACGCAAGTGACATCT-3′
H371A		5′-ACACCGGTGCTGCTCGCAGACCATGATGAGCGGC-3′

[a]Altered nucleotides are underlined.

known for this enzyme (*13*). Most importantly, we verified these calculated results by site-directed mutagenesis.

MATERIALS AND METHODS

Expression of pACY1 in E. coli—Total RNA was extracted from porcine kidney by a single-step RNA isolation method (*14*). The cDNA was amplified by RT-PCR from the total RNA using a SMART™ cDNA synthesis kit (Clontech). The gene encoding pACY1 was amplified by PCR from the cDNA using Platinum® *Pfx* DNA polymerase (Invitrogen) and the following primers: (a) 5′-TTA*GGATCC*GCCATGGCCAG-3′ and (b) 5′-GGGT*GAATTC*GGAGCTCAGC-3′. The sequences highlighted by italics are the *Bam*HI and *Eco*RI restriction sites used to insert the fragment into the appropriately cut T7 expression vector pET28a. The inserted pACY1 gene in pET28a vector was confirmed by DNA sequencing. For expression, the *E. coli* strains BL21 (DE3) and BL21 Rosetta™ (DE3) (Novagen) were transformed with the resulting plasmid. The cells were grown at 37°C to an A_{600} of 0.8 before expression was induced by addition of IPTG (0.2 mM final concentration). After an additional 3 h of shaking, the cells were harvested and used for enzyme preparation.

Enzyme Preparation—The cell pellet was washed with PBS, resuspended in100 mM potassium phosphate buffer, pH 7.0 (KP_5O_7), and disrupted by sonication. The supernatant was purified as described (*15*). Protein concentrations were determined by the Bradford assay (*16*) with bovine serum albumin as the standard.

SDS-PAGE—Protein were separated in 12% SDS-PAGE. When dilute solutions were to be analyzed, the proteins were concentrated by precipitation with TCA. The pellet was taken up in sample buffer and neutralized with Tris base before loading. The gels were stained with either Coomassie Blue R-250 or silver stain.

Aminoacylase I Assays—Aminoacylase 1 activity was assayed by determination of L-methionine released in the reaction using the colorimetric ninhydrin method (*10*). Native pACY1 (Fluka) was used as a control to evaluate recombinant enzymes. One unit of ACY1 is defined as the amount of enzyme that hydrolyzes 1 μmol of *N*-acetyl-L-methionine per minute at 25°C. Kinetic data were evaluated by nonlinear regression analysis, using the Michaelis–Menten equation ($v = V_{max}*[S]/K_m + [S]$). The "melting temperature" Tm of each enzyme variant was determined as reported (*15*).

Site-Directed Mutagenesis—Site-directed mutagenesis was performed on the vector pET28a using a QuikChange™ site-directed mutagenesis kit (Stratagene). Forward versions of mutagenic primers were listed in Table 1. The mutant pACY1 genes in the expression vectors were confirmed by DNA sequencing. All mutants were expressed in Rosetta™ (DE3) strains.

Circular Dichroism Spectra—CD spectra were recorded at 20°C with 0.5 mg/ml of enzyme in 0.1 M (pH 7.0) sodium phosphate buffer in Jasco J720 spectrometer.

Structure-Based Alignment—Structure-based alignments were derived between the structure of CPG2, and one zinc-binding domain in the T347G mutant of hACY1, and the dimerization domain of nmDAPE using the identical homologous residues. Models of the compared proteins were fitted, and RMSD calculations were performed for Ca atoms.

Homology Modeling—The optimized homology model of pACY1 was built with the program MODELLER 7v7 (*17*). The pACY1 sequence (SWISS-PROT entry P37111) was used as a target, and the structure of CPG2 (*18*) (chain A and chain D of PDB entry 1CG2), zinc-binding domain of the T347G mutant of hACY1 (*8*) (PDB entry 1Q7L), and nmDAPE (PDB entry 1VGY) as the templates. The sequence alignments were carried out with CLUSTALW version 1.82 (http://www.ebi.ac.uk/clustalw/) using default parameters. Secondary structure information for the target and structure alignments were derived from 3D-PSSM predictions (http://www.sbg.bio.ic.ac.uk/3dpssm/). Both aligned results were adjusted manually to minimize the number of gaps and insertions.

Because of discrepancies with the template in the zinc-binding site regions, zinc ions and zinc-binding water molecules from the X-ray structures were excluded in the template. MODELLER calculations included secondary structure restraints for helical and strand regions in the dimerization domains, and distance restraints for the single zinc ion of each subunit (*12*, *13*, *19*).

Fifty MODELLER models were generated from the alignment. The models that exhibited no topological errors were analyzed with PROCHECK3.5 (*20*). The best models from PROCHECK analysis were then underwent energy minimization after adding water molecules and counter ions with the SANDER module of AMBER 7 (*21*), using the PARM99 force field (*22*), an additional force field for zinc ion (*23*), a dielectric constant of 1.0, and a 12 Å cutoff for non-bonded interactions. The minimization protocol

included 100 steps of steepest descent, followed by 2000 steps of conjugate gradients. Validation of the final model was obtained with PROCHECK3.5 and PROSA2003 (*24*).

Docking Using AutoDock3.05—*N*-Acetyl-L-methionine, the best substrate of pACY1 (*13*), was used as the ligand to dock. AutoDockTool (ADT) was used to prepare the docking files. Zinc parameters (zinc radius: 0.87 Å; well depth: 0.35 kcal/mol; and zinc charges: +0.95 e) were used in the docking files (*25*).

AutoDock3.05 (*26–28*) offers an option of three search algorithms to explore the space of active binding with different efficiencies. We used the Lamarckian genetic algorithm in this study. The docking was performed in two steps. The first step is to position the ligand in the model. To achieve this, we set a grid centered on the model. The second step is to find the plausible dockings. For this purpose, the grid size was set to 120 × 120 × 120 points with a grid spacing of 0.5 Å centered on the ligand. The grid box included the entire structure of the model and provided enough space for translational and rotational walk of the ligand. The maximum number of energy evaluations was set to 10 million, and 150 independent runs were performed. For each of the 150 independent runs, a maximum number of 27,000 GA operations were generated on a single population of 100 individuals. The parameters not described in detail here were set to default by the program.

RESULTS AND DISCUSSION

Expression of pACY1—To obtain enough pACY1 for enzymatic study, the pACY1 cDNA was reverse-transcribed from the total RNA extracted from porcine renal tissue and was amplified with PCR using the primer pair. The PCR amplified cDNA fragment was then restricted by *Bam*HI and *Eco*RI, inserted to the appropriately cut T7 expression vector pET28a, and overexpressed in *E. coli*. The cDNA sequence in our study was confirmed by DNA sequencing and was found to be identical to the reported pACY1 gene (*29*, *30*). As shown in Table 2, pACY1 when overexpressed in *E. coli* strain BL21 (DE3) had a much lower specific activity than the native enzyme.

Since pACY1 overexpressed in *E. coli* strain BL21 had a very low specific activity, the BL21-derived Rosetta™ host strain was also utilized to overexpress this protein in our study. The Rosetta™ host strains contain codons rarely used in *E. coli* to enhance the expression of eukaryotic proteins. Supposedly, pACY1 expressed in the Rosetta™ strains should be correctly translated as in a eukaryotic system and have normal activity. As demonstrated in Table 2, the specific activity of pACY1 overexpressed in the Rosetta™ strains was much higher than that overexpressed in *E. coli* BL21, But it was still lower than the native enzyme. The exact reason for this observed low specific activity of pACY1 overexpressed in both *E. coli* strains remains unclear. It may be due to posttranslational modification of this enzyme. In fact, the alanine residue immediately next to the starter methionine of pACY1 is known to undergo acetylation (*29*). This enzyme also contains two potential glycosylation sites, but the presence of carbohydrate in purified enzyme has not been convincingly demonstrated, and it therefore remains unclear whether glycosylation of this enzyme occurs in our expression system and is responsible for the low specific activity. No other sequence motifs indicative of other posttranslational modifications are present (*13*). Therefore, we suggest that the failure to achieve the optimal

Table 2. **Kinetic parameters for the hydrolysis of *N*[a]-acetyl-L-methionine catalyzed by variant pACY1.**

pACY1 variant	V_{max} (U/mg)	K_m (mM)	T_m (°C)
Native enzyme (porcine kidney)	287 ± 7	0.84 ± 0.04	68
Wild type [BL21 (DE3)]	10.3 ± 0.2	ND[a]	ND
Wild type [Rosetta (DE3)]	220 ± 7	1.25 ± 0.07	65
H79A	6.4 ± 0.3	2.21 ± 0.10	49
D112A	9.4 ± 0.2	2.52 ± 0.15	50
E146A	13.6 ± 0.6	4.34 ± 0.25	60
E147A	25.7 ± 0.7	2.23 ± 0.30	51
E174A	53.6 ± 0.4	2.36 ± 0.20	54
H205L	78.5 ± 1.2	3.82 ± 0.16	60
N261A	9.2 ± 0.2	4.57 ± 0.13	61
R274A	197 ± 5	2.12 ± 0.07	62
R348A	NM[b]	NM	NM
E309H	203 ± 5	1.20 ± 0.04	62
H371A	32.6 ± 0.6	2.45 ± 0.18	55

[a]ND, not determined. [b]NM, not measurable.

Fig. 1. **Stero representation of the zinc-binding domain in the T347G mutant of hACY1 and the dimerization domain in nmDAPE superimposed onto CPG2.** The structures are colored in black, gray and jet-black for hACY1, nmDAPE and CPG2, respectively.

```
pACY1      -------ASKGREGEHPSVTLFRQYLRIRTVQPEPDYGAAVA-FLEERARQLGLGCQKVEVVPGHVVTV   61
1Q7L_ABCD ----------EEEHPSVTLFRQYLRIRTVQPKPDYGAAVA-FFEETARQLGLGCQKVEVAPGYVVTV
1CG2_AD   QKRDNVLFQAATDEQPAVIKTLEKLVNIETGTGDAEGIAAAGNFLEAELKNLGFTVTRSKSAGLVVGDN
1VGY_A1B1 ------------------------------------------------------------------

pACY1      LTWPGTNPTLSSILLNSHTDVVPVFKEHWSHDPFEGFKDADGYIYGRGAQDMKCVSIQYLEAVRRLKVE  130
1Q7L_ABCD LTWPGTNPTLSSILLNSHTDVVPVFKEHWSHDPFEAFKDSEGYIYARGAQDMKCVSIQYLEAVRRLKVE
1CG2_AD   IVGKIKGRGGKNLLLMSHMDTV-YLKGILAKAP---FRVEGDKAYGPGIADDKGGNAVILHTLKLLKEY
1VGY_A1B1 ------------------------------------------------------------------

pACY1      GHHFPRTIHMTFVPDEEVGGHQGMELFVKRPEFQALRAGFALDEGLASPTDAFTVFYSERSPWWLRVTS  199
1Q7L_ABCD GHRFPRTIHMTFVPDEEVGGHQGMELFVQRPEFHALRAGFALDEGIANPTDAFTVFYSERSPWWVRV--
1CG2_AD   GVRDYGTITVLFNTDEEKGSFGSRDLIQEEAKLADYVLSFEP-----TSAGDEKLSLGTSGIAYVQVNI
1VGY_A1B1 ------------------------------------------------------------LSGNLTV

pACY1      TGKPGHGSRFIEDTAAEKLHKVINSILAFREKEKQRLQSNQLKPGAVTSVNLTMLEGGV-AYNVVPATMS  268
1Q7L_ABCD ------------------------------------------------------------------
1CG2_AD   TGKASHA-----GAAPELGVNALVEASDLVLRTMNIDDKAKN-----LRFNWTIAKAGN-VSNIIPASAT
1VGY_A1B1 KGKQGH-----IAYPHLAINPVHTFAPALLELTQEV-WDEGNEYFPPTSFQISNINGGTGATNVIPGELN

pACY1      ACFDFRVAPDVDLKAFEEQLQSWCQAAG-EGVTFEFVQKWMETQVTSTDDSDPWWAAFSGVFKDMKLALE  337
1Q7L_ABCD ----------------------------------------------NPWWAAFSRVCKDMNLTLE
1CG2_AD   LNADVRYARNEDFDAAMKTLEERAQQKKLPEADVKVIVTRGRPAFNAGEGGKKLVDKAVAYYKEAGGTLG
1VGY_A1B1 VKFNFRFSTESTEAGLKQRVHAILDKH---GVQYDLQWSC-SGQPFLTQAG--------------------

pACY1      LEICPAS-TDARYIRAAGVPALGFSPMNHTPVLLHDHDERLHEAVFLRGVDIYTQLLSALASVPALPSES  406
1Q7L_ABCD PEIMPAA-GDNRYIRAVGVPALGFSPMNRTPVLLHDHDERLHEAVFLRGVDIYTRLLPALASVPALP SDS
1CG2_AD   VEERTGGGTDAAYAALSGKPVIESLGLPG-FGYHSDKAEYVDISAIPRRLYMAARLIMDLGAG-------
1VGY_A1B1 ------------------------------------------------------------------
```

Fig. 2. **Sequence alignment of pACY1, T347G mutant of hACY1, CPG2, and the dimerization domain of DAPE produced by CLUSTALW.** 1Q7L_ABCD represents the chains A, B, C and D in 1Q7L. The 4 amino acids absent in 1Q7L_CD are indicated in italics. The structures of 1Q7L_AB and 1Q7L_CD were used as templates to model the different catalytic domains of pACY1. 1CG2_AD represents chain A and chain D in 1CG2; 1VGY_A1B1 represents the dimerization domains of chain A and chain B in 1VGY.

specific activity in the Rosetta™ (DE3) expression system is due to unsatisfactory processing of the N-terminus of the primary transcript. However, using pACY1 prepared from the Rosetta™ (DE3) expression system, we were able to obtain fair catalytic parameters (V_{max}: 220 ± 7 U/mg and K_m: 1.25 ± 0.07 mM) when compared with the native enzyme (V_{max}: 287 ± 7 U/mg and K_m: 0.84 ± 0.04 mM). Therefore, the Rosetta™ (DE3) expression system was applied to express the wild type and mutants of pACY1 in this study.

Structure-Based Alignment—The structures of the zinc-binding domain in the T347G mutant of hACY1 and nmDAPE are similar to the structure of CPG2. Because these three enzymes are all homologous oligomers, the structure-based alignments were done with their monomer structures (Fig. 1). The superposition of the zinc-binding domain in the T347G mutant of hACY1 on the catalytic domain of CPG2 overlaps 201 Ca atoms out of 263 with an RSMD of 1.53. Given the similar secondary structure elements, the broken parts of the zinc-binding domain in the T347G cannot fit well with CPG2. The degradation of the dimerization domains of hACY1 before it forms crystals can change the conformation of these secondary structures. The structure of nmDAPE is present as a zinc-free form. Therefore, the dimerization domain of this structure was selected as a template instead the whole structure. And the superposition of the dimerization domain of nmDAPE on the corresponding domain of CPG2 overlaps 94 Ca atoms out of 116 with an RSMD of 1.41.

Homology Modeling—ACY1 is a homodimeric protein. Each monomer contains a catalytic domain and a dimerization domain. pACY1 and hACY1 are closely related and share a sequence identity of 87.7% at the amino acid level (*4*). Recently Linder and his collaborators illustrated the crystal structure of the zinc-binding domain (also called the catalytic domain) of the T347G mutant of hACY1 and suggested that catalysis in hACY1 occurs at the dimer interface (*8*). Therefore, in order to probe the catalytic center and to understand the catalytic mechanism of pACY1, the dimeric structure of pACY1 is required. In this work, we chose the crystal structure of CPG2, a polymeric protein that is significantly homologous to pACY1 in sequence and structure, as another template. Considering the relatively low level of sequence identity (~20%) within the dimerization domains of pACY1 and CPG2, we based on the alignment of the dimerization domains, which had been verified by the cross-linking experimental data (*9*), and used the dimerization domains of the crystal structure of nmDAPE as the supplementary template. The final alignment is shown in Fig. 2.

The number of zinc ions within the catalytic subunit is different between the target and templates (one for pACY1, two for CPG2 and hACY1) (*8*, *12*, *13*, *18*, *19*). The binuclear zinc coordination of hACY1 is very similar to that of CPG2. However, the two zinc-binding amino acid residues, His^{385} and Glu^{200} in CPG2, are not conserved in the multiple alignments with other aminoacylases (*9*). The data of site-directed mutagenesis described below also indicated that the metal coordination in pACY1 involves ASP^{112}, His^{79}, and Glu^{147}, as proposed by Biagini and Puigserver (*31*).

After PROCHECK analyses, the best two models (model A and B) from fifty models underwent an energy minimization procedure. Model validation of the minimized structures (model A1 and B1) was performed with PROCHECK and PROSA analysis. These values of model B1 (PROCHECK G-factor: from –0.21 to –0.03 and PROSA pair energy: from –1.87 to –0.25) were quite satisfactory for

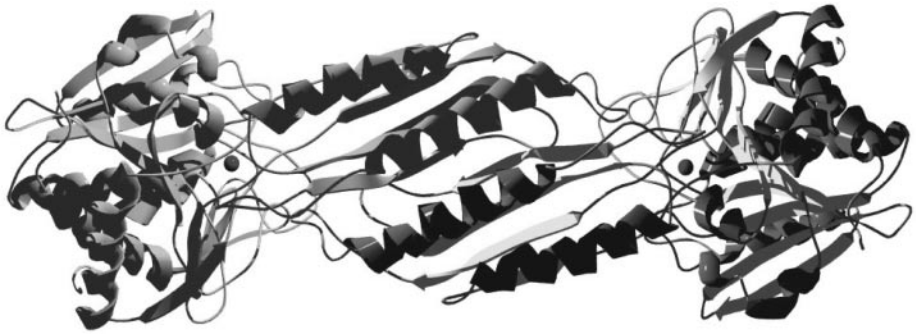

Fig. 3. **Ribbon representation of the final pACY1 model.** The backbone of Model B1 is colored by secondary structure. The zinc ion is represented as the black sphere.

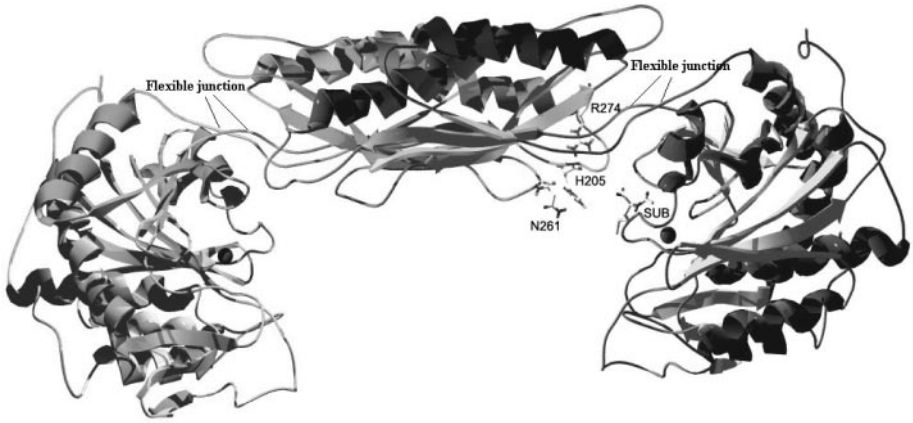

Fig. 4. ***N*-Acetyl-L-Met (SUB) docked in the vicinity of the zinc center of pACY1 (Model B1) using Autodock3.05.** The backbone of Model B1 is colored by secondary structure. The zinc ion is represented as the black sphere. SUB is shown in a stick representation.

a structure obtained from homology modeling with templates of relatively low level of sequence identity. From these values, we chose the better model B1 as the final model to perform docking with the substrate. The ribbon diagram of model B1 is shown in Fig. 3. The monomer consists of two domains: the catalytic domain, which is a globular compact subunit that comprises residues 1–188 and 311–406, forming a β-sheet sandwiched between α-helices; and the dimerization domain, which comprises residues 189–310, folding into a β-sheet flanked on one side by two α-helices.

Docking of the Substrate to pACY1—The model B1 obtained from homology modeling was used to dock with *N*-acetyl-L-methionine, the best substrate of pACY1 (*13*). After two-step docking by AutoDock3.05, a reasonable binding mode was obtained through the lowest energy and the frequency of docking poses. As shown in Fig. 4, the substrate was docked into the region near the zinc ion. We noted the distance between the substrate and the zinc atom was more than 6.3 Å, which is too far to allow direct contact between them. Our result therefore supported the previous suggestion that binding of the substrate to pACY1 does not depend on the metal ion (*12*, *15*).

Plausible interactions between the model B1 and the substrate within a contact distance of 4.0 Å were analyzed carefully. As shown in Fig. 5A, two residues, Glu^{146} and Arg^{348}, were found to form hydrogen bonds with *N*-acetyl-L-methionine (SUB). More specifically, the carbonyl group of Glu^{146} is 2.0 Å from the SUB and forms a hydrogen bond with the hydrogen at the amido of SUB; the amine group of Arg^{348} is only 2.75 Å from SUB and forms two hydrogen bonds with the carboxyl and carbonyl groups of SUB. These results suggest that Glu^{146} and Arg^{348} play important roles in substrates binding and catalysis. Interestingly, the hydrogen bond between Glu^{146} and SUB also explains the chiral catalytic character of pACY1.

Characterization of pACY1 Mutants—All of the mutants in this work (Table 1) showed the same expression and purification behavior as the wild-type enzyme. On SDS-PAGE, the mutant and wild-type enzymes appeared almost homogenous after passage through the Q-Sepharose column (Fig. 6). Effects of the mutations on protein stability and catalytic activity were investigated (Table 2).

To validate the modeling zinc coordination, we mutated the relevant residues of pACY1 (His^{79}, Asp^{112}, Glu^{147}, Glu^{174}, and His^{371}) that are conserved and are binuclear zinc-ligands in hACY1 (Fig. 7). All five mutants of these residues, H79A, D112A, E147A, E174A, and H371A, had significantly reduced specific activity and protein stability (Table 2). Specifically, the specific activity of mutants H79A, D112A, and E147A was down to 3% of that of the wild-type enzyme, and that of mutants E174A and H371A was down to 15%. The "melting temperature" T_m of H79A, D112A, and E147A was reduced by 14–16°C, while that of E174A and H371A was reduced by 10–11°C. The substrate concentration at half-saturation, which is given by the K_m

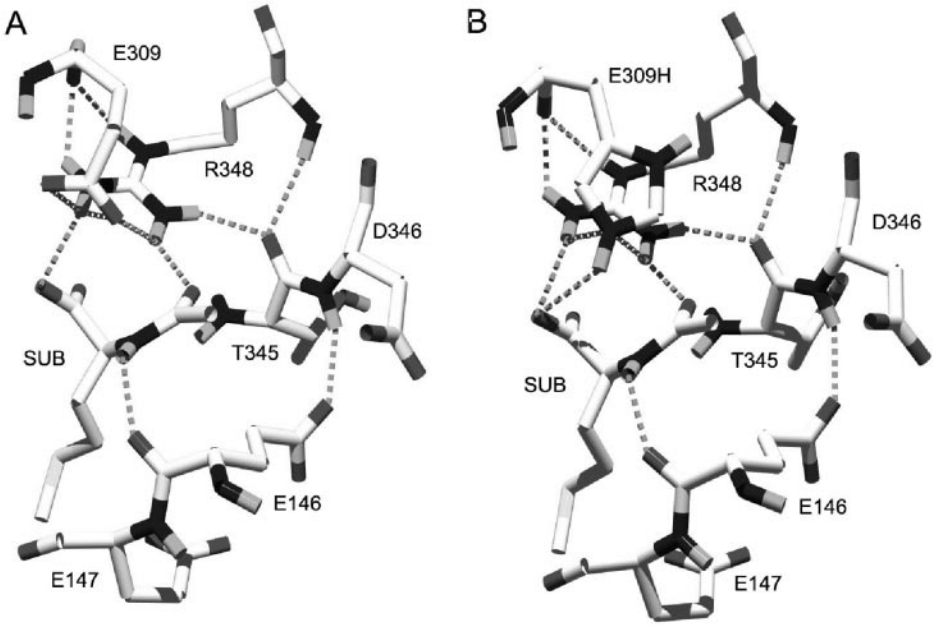

Fig. 5. **Plausible interaction between the model and the substrate (SUB) within a contact distance of 4.0 Å.** Hydrogen bonds are represented by gray dotted lines. (A) The hydrogen bonds between the model B1 and SUB. (B) The hydrogen bonds between the model of E309H and SUB.

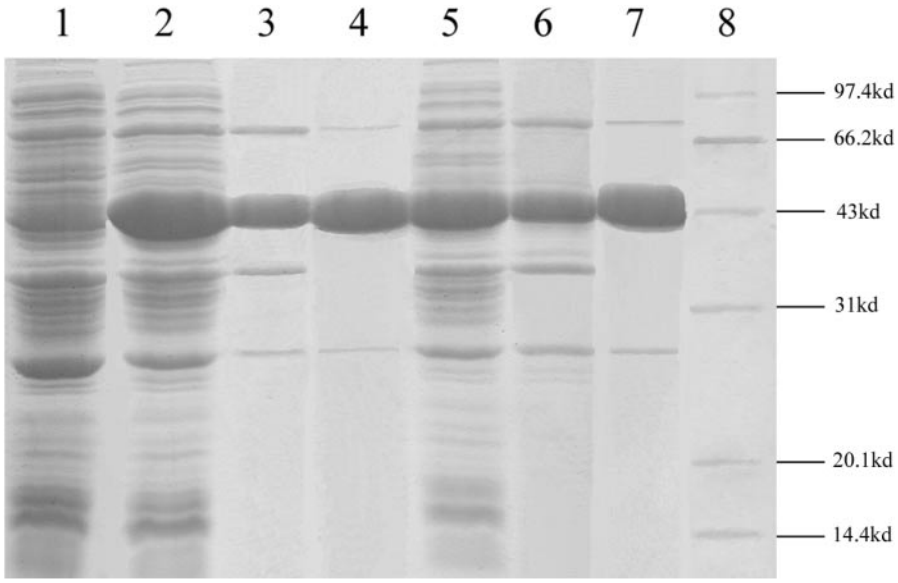

Fig. 6. **Analysis by SDS-PAGE of fractions obtained during purification of recombinant pACY1 from Rosetta (DE3).** Lane 1, extract of the cells transformed by empty pET28a; lane 2, crude cell extract as wild type; lane 3, phenyl-Sepharose elute of wild type; lane 4, Q-Sepharose elute of wild type; lane 5, crude cell extract as variant mutants (R348A used as the representation); lane 6, phenyl-Sepharose elute of R348A; lane 7, Q-Sepharose elute of R348A; lane 8, protein marker.

values obtained from the Michaelis-Menten equation, increased up to 2-fold for these five mutants. These data indicate that the three residues (His^{79}, Asp^{112}, and Glu^{147}) are more important than Glu^{174} and His^{371} and are involved in the zinc coordination of pACY1. As to the fourth coordination site of zinc, which was not modeled in our models, it is well known that, in metalloproteases, it is occupied by a water molecule, which in turn interacts with an acidic residue via hydrogen bonding (*18*, *32*). In our model, the above five residues were within the 4.0 Å from the zinc ion (Fig. 7). The decreased activity and T_m of these five mutants are additional evidence suggesting that the conformation of the zinc center contains a more ordered structure, and the presence of a zinc ion helps to maintain the conformation of the active site (*33*). Glu^{174} and His^{371} in pACY1, which are not highly conserved in the multiple alignments with other aminoacylases (*9*), may form a second metal-binding site of low affinity with Asp^{112}, and upon dialysis, the metal occupying the low-affinity site is lost, as DAPE (*34*). The mutations E174A and H371A should therefore also damage the enzyme activity and stability. However, there are no reported data demonstrating pACY1 having two zinc ions per subunit, and detailed X-ray crystallography studies are needed to confirm it in the future.

In Model B1, we observed that the residue Glu^{146} could act as an acidic residue (*8*, *18*, *32*) that interacts with zinc-binding water, so we produced the mutant E146A. E146A showed a 20-fold decrease in enzyme activity and a 4-fold increase in K_m (Table 2). This confirmed that Glu^{146} is

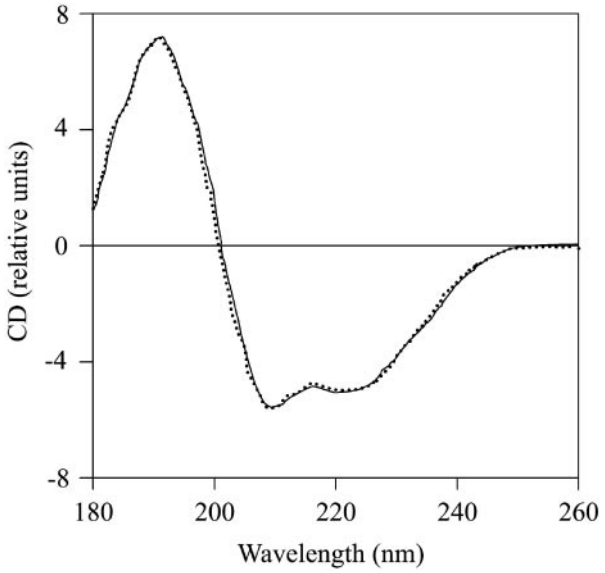

Fig. 7. **CD spectra of wild type pACY1 (–) and R348A (···).** The enzymes were dissolved in 0.1 M (pH 7.0) sodium phosphate buffer at the same protein concentration.

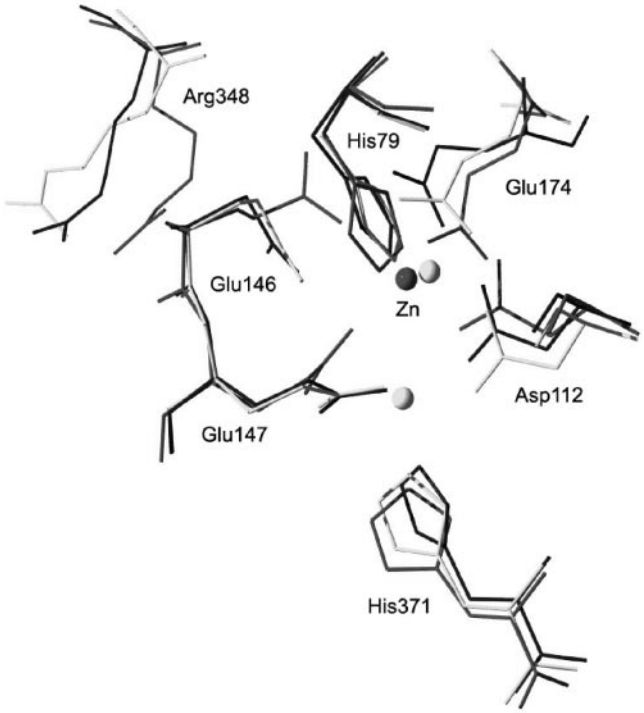

Fig. 8. **Superposition of the plausible catalytic centers of pACY1, hACY1 and nmDAPE.** The structures were colored in jet-black, gray and black for pACY1, hACY1 and nmDAPE, respectively. The numbering is given for pACY1.

involved not only in catalytic activity but also substrate binding, as shown in Fig. 5.

Because the docking study suggested a possible role for Arg^{348}, mutant R348A was produced, which was found to have no detectable activity (Table 2). Furthermore, possible effects of R348A on the integrity of the protein conformation were investigated by CD spectroscopy (Fig. 7). The spectrum of R348A was as same as that of the wild-type enzyme, and the contents of different secondary structures were estimated by the method of Johnson (*35*) (α-helix: 32%; β-sheet: 19%; turn and coil: 49%). The CD assays showed that the loss of activity of R348A is not caused by disruption of the secondary structure. The results suggest that Arg^{348} is essential for activity and plays an important role in catalysis. As shown in Fig. 5A, the amine group of Arg^{348} forms an important hydrogen bond with carbonyl group of SUB. Arg^{348} polarizes the carbonyl of the substrate, allowing the water nucleophile to attack efficiently. A similar role of arginine has been reported in one of the catalytic mechanisms of metalloproteases (*36*). There are 29 different residues between pACY1 and hACY1, distributing all over the proteins. Among these, the greatest discrepancy is Glu^{309} in pACY1, in the vicinity of the catalytic center, forming two hydrogen bonds with Arg^{348} (Fig. 5A), which is replaced by histidine in hACY1. So, we made the mutant E309H, and got similar kinetic parameters to the wild enzyme (Table 2). After simulation of site-directed mutagenesis, further docking was done as described for model B1. As shown in Fig. 5B, the substrate was docked in the same position as before, and the hydrogen-bond interactions between this residue and Arg^{348} were hardly changed after mutating glutamic acid to histidine. The data of mutant E309H further confirmed the docking result and indicated that pACY1 and hACY1 have a same catalytic pattern. Based on these data, we propose that the catalytic center of pACY1 contains Arg^{348}, the whole zinc center, and Glu^{146}.

We also mutated individually each of the three highly conserved residues in the dimerization domains of pACY1 (His^{205}, Asn^{261} and Arg^{274} as shown in Fig. 4). The specific activities of H205L and N261A were reduced to 35% and 4% of wild-type enzyme respectively, while the mutant R274A had relatively normal activity (Table 2). The K_m values increased one fold for R274A and more than two fold for H205L and N261A. These three mutations did not greatly affect the protein stability, as judged from the changes of T_m. Compared with H205L and N261A, R274A affected catalysis less, and the role of Arg^{274} will not be discussed in detail. His^{205} and Asn^{261} in pACY1, which are homologous to His^{206} and Asn^{263} in hACY1, were thought to be brought into the vicinity of the zinc center from the opposite monomer by a conformational change upon substrate binding; especially, His^{205} was indicated to contribute in trans to the active site in the complementation assay (*8*). D'Ambrosio *et al.* calculated the solvent accessibility of Glu^{309} and Gln^{311} in pACY1 and suggested that the junction region between the catalytic domain and the dimerization domain is flexible, and a conformational change in this region changes relative orientation of the two domains (*9*). Comparing the structures of CPG2, nmDAPE, PepT and PepV, we found that they are largely very similar, including the secondary structure elements, and that they differ only in the relative orientations of the catalytic domain and the dimerization domain. This supports the notion that pACY1 and hACY1 have a flexible junction (Fig. 4), and a conformational change in this region can bring the catalytic domain close to the dimerization domain. His^{205} and Asn^{261} in model B1 are

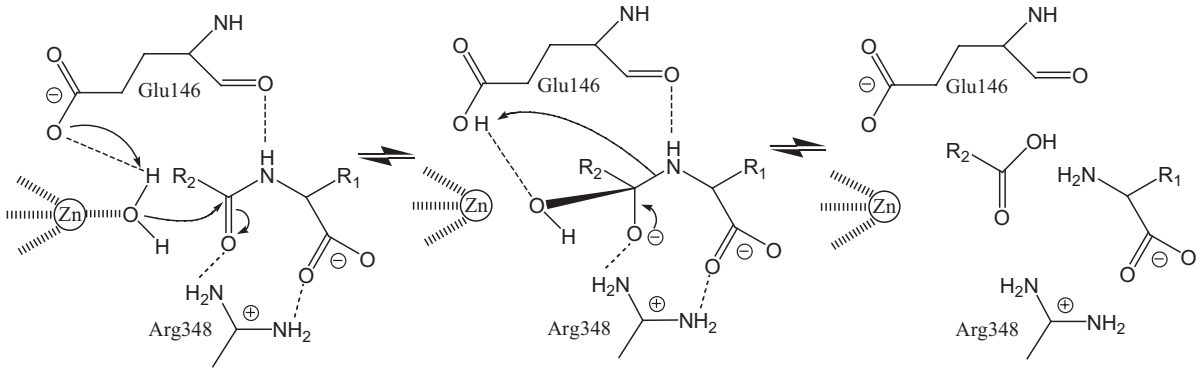

Fig. 9. **Proposed enzyme mechanism of ACY1 and DAPE.** Glu^{146} (numbering according to pACY1) acts as a general base and accepts a proton from the metal-bridging water nucleophile (*8*, *18*, *32*). The proton is shuttled to the leaving amino group to facilitate breakdown of the tetrahedral intermediate. Arg^{348} (numbering according to pACY1) acts as an anchor in favor of nucleophilic attack by hydroxide and can stabilize the tetrahedral intermediate.

solvent-exposed and close to each other at a distance of 4.0 Å, as are the homologous histidine and asparagine in the crystal structures of CPG2 and nmDAPE. Furthermore, the polar side chains of these two residues extend in the same direction (Fig. 4) and easily capture the substrate in the solution together. The increase in K_m of H205L and N261A supports the idea that these two residues are involved in the substrate binding. Based on the present mutagenesis results and the structural similarity between the members of M20 family and pACY1, the roles of His^{205} and Asn^{261} are suggested to bind with the substrate in solution and to transport the substrate to the catalytic center of pACY1 by the conformational change in the inter-domain interfaces, or to transfer the products from the catalytic center to solution. It remains to be tested whether His^{205} and Asn^{261} are directly involved in catalysis.

Similar Structures of pACY1, hACY1 and DAPE—Interestingly, an arginine residue homologous to Arg^{348} of pACY1 is present at a similar position in the crystal structure of nmDAPE. This arginine is conserved in the multiple alignments with various kinds of DAPE (*34*). In Fig. 7, we superimposed the suggested catalytic center of pACY1 over the structures of hACY1 and DAPE on the basis of amino acid residues. An RSMD of less than 0.47 Å for the Ca atoms of these residues indicates that the catalytic centers are identical within the error limits of the atomic coordinates. Furthermore, pACY1 and DAPE have other similar properties, including substrate specificities, metal contents, and pH dependence (*30*, *34*, *37*, *38*). Especially, DAPE exhibits ~80% of its total activity after binding only one zinc ion (*37*). Thus, we hypothesize that ACY1 and DAPE share a similar catalytic mechanism.

Enzyme Mechanism—The zinc ion in ACY1 is reported to act to stabilize the active conformation (*33*) and not to be involved in substrate binding (*12*, *15*). Furthermore, in our work, Arg^{348} in pACY1 is essential for enzyme activity, which has not been reported before. All of these data suggest that ACY1 has a new enzymatic mechanism. Base on the data in this work, we propose a revised enzymatic mechanism for pACY1 (Fig. 8). Substrate binding is accompanied by coordination of the substrate to Glu^{146} and Arg^{348} as shown in Fig. 5. The positive charges of Arg^{348} attract the substrate to bind and further stabilize the binding. The substrate is brought into the vicinity of Glu^{146} by the hydrogen bond between the amido of substrate and the carbonyl group of Glu^{146}. The residue Glu^{146} functions as a general base accepting a proton from the zinc-binding water, and the hydroxide attacks the carbonyl of the substrate polarized by Arg^{348} to form a tetrahedral intermediate. Furthermore, formation of the tetrahedral intermediate results in a buildup of negative charge on the oxygens. this negative charge can partly be distributed to the amide nitrogen, which facilitates the proton binding with Glu^{146} transfer to the amide nitrogen and makes the tetrahedral intermediate collapse to form products. However, proton movements may not be unique. For example, water molecules may be involved in the proton transfer paths.

In this revised enzymatic mechanism, the role of the zinc ion is to supply water nucleophile and to stabilize the active center. Whether the number of zinc ions in the subunit of pACY1 is one or two, is not necessary for catalysis. The residue Glu^{146} functions as a general base accepting a proton from the zinc-binding water nucleophile and shuttling the proton to the leaving group. To our knowledge, a similar role of glutamate residues has been proposed in other metalloproteases (*8*, *18*, *34*, *39*). Coordination of the residue Arg^{348} to the substrate provides favorable polarization of the carbonyl and orientation for a nucleophilic attack by the hydroxide.

In conclusion, we have characterized the structural and functional properties of the presumed enzyme-substrate complex structure of pACY1 by homology modeling and substrate docking. The modeling and docking results were further confirmed by our experimental data. A revised enzymatic mechanism of amide bond hydrolysis, which may be shared by pACY1, hACY1 and DAPE, is proposed. The results presented in this paper can also be an example of a means to probe the catalytic center of those enzymes without structural information.

The present study was supported by the National Key Project of Science and Technology (project 2001BA708B02-04) and the National Natural Science Foundation of China (project 39570370). We wish to thank Prof. James W. Caldwell of the University of California for offering us the AMBER 7.

REFERENCES

1. Wang, HR., Zhang, T., Wang, ZF., Wang, XC., and Zhou, HM. (1995) Aminoacylase from pig kidney contains no disulfide bonds. *Sci. China Ser. B* **38**, 1448–1454
2. Palm, G.J. and Röhm, K.H. (1995) Aminoacylase 1 from porcine kidney: Identification and characterization of two major protein domains. *J. Protein Chem.* **14**, 233–240
3. Tsunasawa, S., Narita, K., and Ogata, K. (1975) Purification and properties of acylamino acid-releasing enzyme from rat liver. *J. Biochem.* **77**, 89–102
4. Mitta, M., Kato, I., and Tsunasawa, S. (1993) The mucleotide sequence of human aminoacylase-1. *Biochimica et Biophysica Acta* **1174**, 201–203
5. Tsunasawa, S. (1992) Does uncontrolled survival of acetylated peptides lead to cell proliferation? Deletion of N-terminal deacetylating system for protein/peptide in small lung carcinoma cells. *J. Lab. Clin. Med.* **120**, 505–506
6. Scaloni, A., Jones, W.M., Pospischil, M., Schneewind, O., Popowicz, A., Bossa, F., Graziano, S., and Manning, J.M. (1992) Deficiency of acylpeptide hydrolase in small-cell lung carcinoma cell lines. *J. Lab. Clin. Med.* **120**, 546–552
7. Zhao, H.Y., Meng, W.Y., Lin, Z.J., and Zhou, H.M. (1997) Crystallization and preliminary X-ray studies of porcine kidney aminoacylase 1. *Chin. Sci.e Bull.* **42**, 1750–1752
8. Lindner, H.A., Lunin, V.V., Alary, A., Hecker, R., Cygler, M., and Ménard, R. (2003) Essential roles of zinc ligation and enzyme dimerization for catalysis in the aminoacylase-1/M20 family. *J. Biol. Chem.* **278**, 44496–44504
9. Ambrosio, C.D., Talamo, F., Vitale, R.M., Amodeo, P., Tell, G., Ferrara, L., and Scaloni, A. (2003) Probing the dimeric structure of porcine aminoacylase 1 by mass spectrometric and modeling procedures. *Biochemistry* **42**, 4430–4443
10. Szajáni, B., Kiss, A., and Boross, L. (1980) Investigation of the active center and catalytic mechanism of porcine kidney aminoacylase: A model of the active center. *Acta Biochim. Et Biophys. Acad. Sci. Hung.* **15**, 29–37
11. Denton, P. (2000) A structure-activity relationship for the hydrolysis of acetylamino acids by porcine aminoacylase. *Bioorg. Chem.* **28**, 205–213
12. Heese, D., Berger, S., and Röhm,K.H. (1990) Nuclear magnetic relaxation studies of the role of the metal ion in Mn^{2+}-subtituted aminoacylase 1. *Eur. J. Biochem.* **188**, 175–180
13. Pittelkow, S., Lindner, H., and Röhm, K.H. (1998) Human and porcine aminoacylase 1 overproduced in a baculovirus expression vector system: evidence for structural and functional identity with enzymes isolated from kidney. *Protein Expr. Purif.* **12**, 269–276
14. Nagamine, T., Aminov, R.I., Sugiura, M., Ogata, K., Tajima, K., and Benno, Y. (1997) Tissue homogenization as a key step in extracting RNA from human and rat pancreatic tissue. *BioTechniques* **22**, 408–412
15. Lindner, H., Berens, W., Kraus, I., and Röhm, K.H. (2000) Mutational analysis of two PWW sequence motifs in human aminoacylase 1. *Biol. Chem.* **381**, 1055–1061
16. Bradford, M.M. (1976) A rapid and sensitive method for the quantitation of protein utilizing the principle of protein-dye binding. *Anal Biochem.* **72**, 248–254
17. Sali, A. and Blundell, T.L. (1993) Comparative protein modeling by satisfaction of spatial restraints. *J. Mol. Biol.* **234**, 779–815
18. Rowsell, S., Pauptit, R.A., Tucker, A., Melton, R.G., Blow, D.M., and Brick, P. (1997) Crystal structure of carboxypeptidase G_2, a bacterial enzyme with applications in cancer therapy. *Structure* **5**, 337–347
19. Kördel, W. and Schneider, F. (1977) Renal aminoacylase 1, a zinc enzyme. *Z. Naturforsch.* **32c**, 342–344
20. Laskowski, R.A., MacArthur, M.W., Moss, D.S., and Thornton, J.M. (1993) PROCHECK: a program to check the stereo chemical quality of protein structures. *J. Appl. Crystallogr.* **26**, 283–291
21. Case, D.A., Pearlman, D.A., Caldwell, J.W., Cheatham III, T.E., Wang, J.M., Ross, W.S., Simmerling, C., Darden, T., Merz, K.M., Stanton, R.V., Cheng, A., Vincent, J.J., Crowley, M., Tsui, V., Gohlke, H., Radmer, R., Duan, Y., Pitera, J., Massova, I., Seibel, G.L., Singh, U.C., Weiner, P., and Kollman, P.A. (2002) *AMBER 7*, University of California, San Francisco
22. Wang, J., Cieplak, P., and Kollman, P.A. (2000) How well does a restrained electrostatic potential (RESP) model perform in calculating conformational energies of organic and biological molecules? *J. Comput. Chem.* **21**, 1049–1074
23. Pang, Y.P., Xu, K., Yazal, J.L., and Prendergast, F.G. (2000) Successful molecular dynamics simulation of the zinc-bound farnesyltransferase using the cationic dummy atom approach. *Protein Sc.* **9**, 1857–1865.
24. Sippl, M.J. (1993) Boltzmann's principle, knowledge based mean fields and protein folding, An approach to the computational determination of protein structures. *J. Comp. Aided Mol. Des.* **7**, 473–501
25. Hu, X. and Shelver, W.H. (2003) Docking studies of matrix metalloproteinase inhibitors: zinc parameter optimization to improve the binding free energy prediction. *J. Mol. Graph. Model.* **22**, 115–126
26. Goodsell, D.S. and Olson, A.J. (1990) Automated docking of substrates to proteins by simulated annealing. *Protein: Struct. Func. Genet.* **8**, 195–202
27. Morris, G.M., Goodsell, D.S., Huey, R., and Olson, A.J. (1996) Distributed automated docking of flexible ligands to proteins: Parallel applications of Autodock 2.4. *J. Computer-Aided Mo. Design* **10**, 293–304
28. Morris, G.M., Goodsell, D.S., Halliday, R.S., Huey, R., Hart, W.E., Belew, R.K., and Olson, A.J. (1998) Automated docking using a Lamarckian genetic algorithm and an empirical binding free energy function. *J. Comp. Chem.* **19**, 1639–1662
29. Mitta, M., Ohnogi, H., Yamamato, A., Kato, I., Sakiyama, F., and Tsunasawa, S. (1992) The primary structure of porcine aminoacylase 1 deduced from cDNA sequence. *J. Biochem.* **112**, 737–742
30. Jakob, M., Miller, Y.E., and Röhm, K.H. (1992) Cloning and sequence analyses of cDNAs encoding aminoacylase 1 from porcine kidney. *Biol. Chem. Hoppe-Seyler* **373**, 1227–1231
31. Biagini, A. and Puigserver, A. (2001) Sequence analysis of the aminoacylase-1 family. A new proposed signature for metalloexopeptidases. *Comp. Biochem. Physiol. Part B.* **128**, 469–481
32. Alberts, I.L., Nadassy, K., and Wodak, S.J. (1998) Analysis of zinc binding sites in protein crystal structures. *Protein Sci.* **7**, 1700–1716
33. Tang, ZY., Yu, JY., Zhou, Q., He, B., Wang, ZF., and Zhou, HM. (1995) Secondary structure of holo- and apo-aminoacylase from predication, circular dichroism, and ft-raman spectroscopy. *J. Biochem.* **118**, 706–709
34. Born, T.L., Zheng, R.J., and Blanchard, J.S. (1998) Hydrolysis of N-Succinyl-L,L-Diaminopimelic acid by the *Haemophilus influenzae dapE*-encoded desuccinylase: Metal activation, solvent isotope effects, and kinetic mechanism. *Biochemistry* **37**, 10478–10487
35. Compton, L.A. and Johnson, W.C. (1986) Analysis of protein circular dichroism spectra for sencondary structure using a simple matrix multiplication. *Anal. Biochem.* **155**, 155–167
36. Hernick, M. and Fierke, C.A., (2005) Zinc hydrolases: the mechanisms of zinc-dependent deacetylases. *Arch. Biochem. Biophys.* **433**, 71–84

37. Bienvenue, D.L., Gilner, D.M., Davis, R.S., Bennett, B., and Holz, R.C. (2003) Substrate specificity, metal binding properties, and spectroscopic characterization of the DAPE-encoded N-succinyl-L,L-diaminopimelic acid desuccinylase from *Haemophilus influenzae*. *Biochemistry* **42**, 10756–10763
38. Galaev, I.Y. and Svedas, V.K. (1982) A kinetic study of hog kidney aminoacylase. *Biochim. Biophy. Acta* **701**, 389–394
39. Javid-Majd, F. and Blanchard, J.S. (2000) Mechanistic analysis of the argE-Encoded N-acetylornithine deacetylase. *Biochemistry* **39**, 1285–1293